

THESIS

**Baseline Compensation System
for Underground Gravitational-wave
Telescope**

Koseki Miyo

*Department of Physics
University of Tokyo*

MMM 2020

Contents

1	Underground Seismic Noise	5
1.1	Seismic Noise	5
1.1.1	Overview	5
1.1.2	Human activity	6
1.1.3	Microseisms	6
1.1.4	Large Earthquakes	7
1.1.5	Earth Tides	8
1.2	Long-term Study of the seismic environment at KAGRA	9
1.2.1	Overview	9
1.2.2	Experimental Arrangement	9
1.2.3	Data	10
1.2.4	Results	11
1.3	Differential Motion Reduction	12
1.3.1	Introduction	12
1.3.2	Differential Motion Reduction	12
1.4	Measurement of Differential Motion Reduction	14
1.4.1	Overview	14
1.4.2	Reduction in X-arm Scale	14
1.4.3	Reduction in Other Short Scale	15
1.5	Summary of the Chapter	16

Chapter 1

Underground Seismic Noise

1.1 Seismic Noise

1.1.1 Overview

Seismic noise cause two main problems to the terrestrial gravitational-wave detectors, arised from the detection principle and the working principle of the detector, which described in ??.

First, the noise limits the sensitivity of the detectors in lower frequency especially below 10 Hz. DARM which recieve the gravitational-wave signal is disturbed by the seismic noises whose amplitude spectrum density is empirically kwnon as

$$\sim \frac{10^{-8}}{f^2} \text{ m}/\sqrt{\text{Hz}} \quad (1.1)$$

, where f is a frequency of the spectrum. Therefore, in order to detect the signal in lower frequencies, vibration isolation system to reduce the seismic noise with extream high isolation factor have been developed [1],[2],[3]. In other words, the seinsitivity of the detector is not limited above 10 Hz owing to the such vibration isolation system.

Second, the noise decrease the duty cycle of the detectors because, realistically, it is difficult to reduce the seismic noise below 0.1 Hz. This difficulty means that the motions not adequately isolated disturb the detector which only can work within the limited range.

...

Under ground can resolve these problems. Places under the ground are more quiet than these on the surface of the ground [4]. Especially, the seismic noise of the underground above 1 Hz is effectivly reduced than the noise of the surface [5], because the noises in this band are correlated to human activities such as industrial machinery, cars and trains, or human footsteps [6] and then are able to be eliminated in underground. Forthermore, A laser interferometer gravitational wave antenna with a baseline length of 20 m (LISM) constructed underground have showed the stable performance of the detector resulting the high duty cycle of 99.8 % [7].

...

However, the improvement of the duty cycle of the large scale detectors is small, because the length change of baseline is larger if the baseline is long as described

in §1.3. For example, in case short baseline such as LISM, the whole ground of the detector tend to be moved by the seismic noise, which means the reduction effect of the short baseline. On the other hands, in case long baseline such as KAGRA, this effect is not effectively in lower frequencies especially below 0.1 Hz in case of the km-scale detector.

The problematic seismic noises are listed in 1.1.

Table 1.1: Baseline changes caused by several seismic sources

Sources	Frequency Band [Hz]	RMS Amplitude [μm]	Detail
Human, traffic	> 1	< 1	§1.1.2
Ocean waves (Microseisms)	0.1–0.3	0.1–10	§1.1.3
Large earthquakes	> 0.05	> 100	§1.1.4
Moon, Sun (Earth tides)	$< 1^{-5}$	> 100	§1.1.5

本節ではそれぞれの地面振動について述べる。

1.1.2 Human activity

...
...
...
...

1.1.3 Microseisms

Microseisms which power spectrum has peaks in 50–200 mHz are excited by oceanic waves. These seismic waves can be categorized by the generating mechanism of these [8].

The primary ocean microseisms are generated only in shallow waters in coastal regions. In this regions, the water wave energy can be converted directly into seismic energy either through vertical water pressure variations, or by the impacts of surf on the shores. There are correlation between this microseismic peak and the swell at the beaches was known starting from the data sets studied by [9].

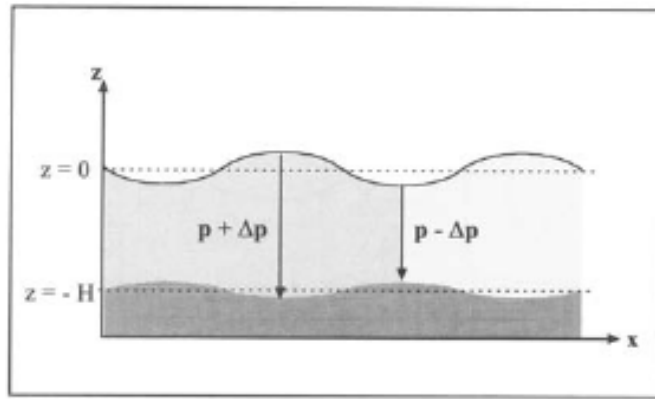
...
...

The secondary ocean microseisms could be explained by the superposition of ocean waves of equal period traveling in opposite directions. Therefore, generating standing gravity waves of half the period [10].

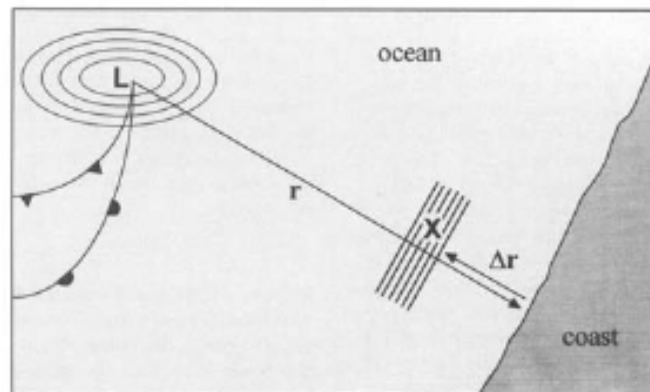
...
...

The RMS amplitude spectral of both type of the microseisms are strongly depends on the low pressure on the ocean [11].

...
...



(a) Generating mechanism of the primary microseisms.



(b) Generating mechanism of the secondary microseisms.

Figure 1.1: Generating mechanism of the microseisms. (a) describes the mechanism of the primary microseisms. (b) describes the mechanism of the secondary microseisms.

1.1.4 Large Earthquakes

hoge

...

...

...

Large amplitude earthquakes around the world would interrupt the operation of the gravitational wave detector and reduce their duty cycle. 実際、観測中に地震でロックが落ちたあと、復帰するまでに数時間かかる場合がある [12]。規模の大きな地震ほど、振幅がおおきいことはもちろん、長周期で減衰までにかかる時間が長い。長周期地震に対して重力波検出器が無効なのは、その防振装置が、せいぜい 100 mHz の地面振動揺れに対して最適化しているためである []。そのためこのような制御方式を使う以上、制御ノイズが増大して感度が落ちることを犠牲にしても、地震が来る前に、地震でロックロスしないような制御フィルターの切り替えを必要とする。この切替のために *Seismon* とよばれる早期地震アラートシステム [13] を用いた制御フィルターの切り替えが試みられている [14]。

hoge

...

...
...

1.1.5 Earth Tides

§1.1.2 hoge

...
...
...

hoge

...
...
...

hoge

...
...
...

1.2 Long-term Study of the seismic environment at KAGRA

1.2.1 Overview

The seismic waves are excited on the source and propagate along the surface of the Earth with amplitude decreasing with depth [4]. However, especially microseisms whose peak is around 0.1 Hz are not attenuated adequately compared with higher frequencies above 1 Hz, because the wavelength is comparable to or longer than the depth. Amount of these attenuation factor is must be explaining by a complicated phenomenon, which depends on either the local geology or location of the exciting sources.

In this section, seasonal change of the RMS amplitude of the seismic noise is described.

1.2.2 Experimental Arrangement

Seismic motion is measured by a seismometer installed on the second floor of the X-end area. This area is placed 200 m underground from the surface of the mountain. Comparison to corner area, human activity in the end area is less because the corner area has parking lots. Comparison to the Y-end area, there is no entrance connected to other mines. Therefore, the X-end area is relatively quiet in the KAGRA mine, regarding the seismic noise induced by human activity.

In this study, Trillium 120-QA which is known as three-component, very broadband, and low-noise seismometer, was used. These three outputs are proportional to the ground velocity of two horizontal and one vertical, respectively. The feature of the low-noise can resolve Peterson's new low-noise model (NLNM) and new high-noise model (NHNM) [15].



Figure 1.2: Trillium 120-QA installed on the second floor at X-end area, which is covered by black thermal insulation cover

As shown in fig 1.2, the seismometer is housed in the black thermal insulation cover according to the installation manual [16]. Thermal insulation protects two broad categories of thermal couplings that can cause unwanted noise [16]. First is the direct coupling to the sensitivity. This coupling typically increases the noise

of the vertical channel as a periodic diurnal variation caused by the day-to-night temperature cycle, because the springs that suspended the inertial masses are temperature sensitive. The second is the coupling to tilt from the thermal fluctuation. Tilt converts the vertical acceleration of gravity into horizontal acceleration. This thermally induced tilt noise on the horizontal will be larger than the direct thermal coupling on the vertical channel. To be low sensitivity to both tilt and temperature, this model has a function to center the inertial mass after the initial installation.

The signals of the seismometer is recorded through the data acquisition system developed by LIGO [17]. The analog signal is converted to digital signal by the 16 bit analog-to-digital converters (ADC) with 16384 Hz sampling. In addition, the signal of the seismoemter is amplified with 30 db so that the ADC noise does not mask this signal.

...

1.2.3 Data

定常な時系列データを1年間のデータのから選んだ。

1.4.

...

...



Figure 1.3: Available data from June 00 2018 to Jun 00 2019

hoge ...

...

...

...

hoge ...

...

...

...

hoge ...

...

...

...

1.2.4 Results

一年間の地面振動スペクトル。...

...

...

...

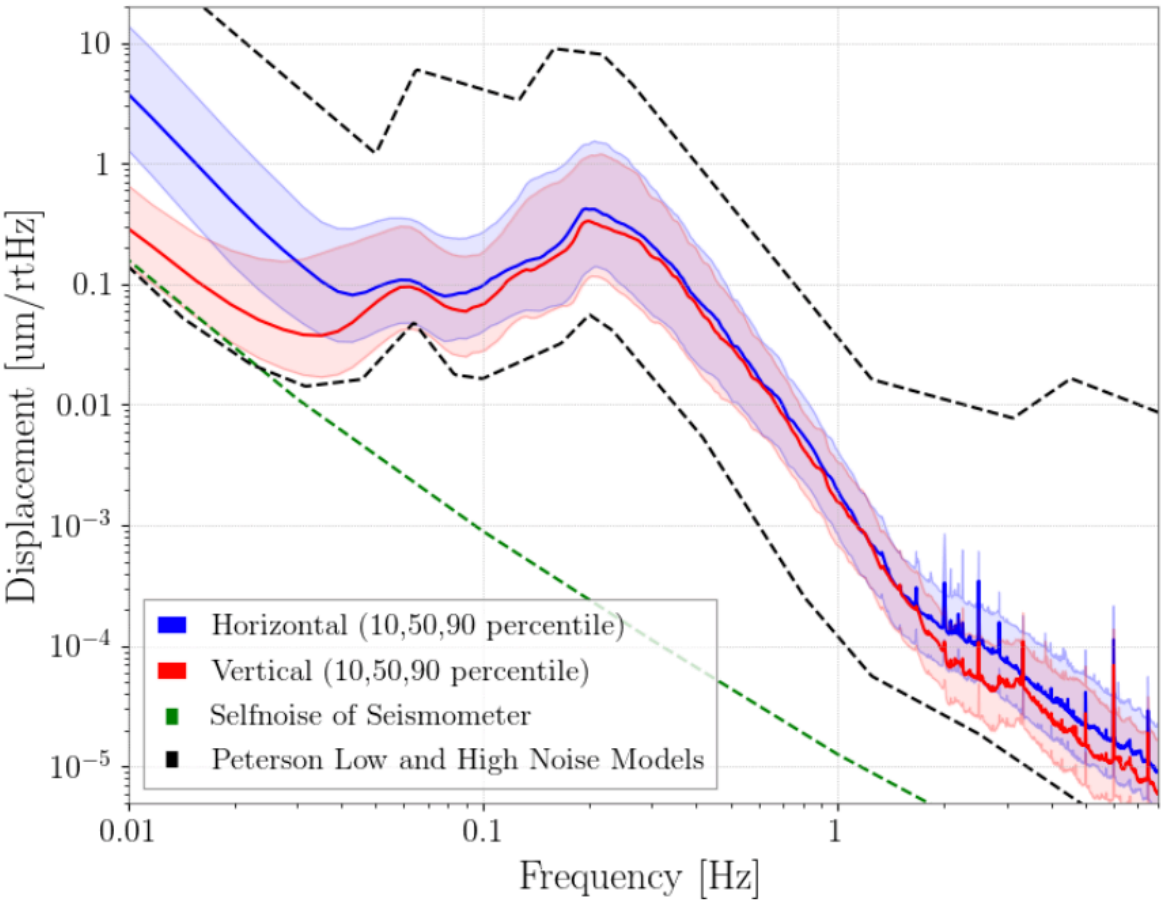


Figure 1.4

地面振動の季節変動。...

...
...
...



NO IMAGE

Figure 1.5

台風の移動と脈動の変化...

...
...
...

1.3 Differential Motion Reduction

1.3.1 Introduction

The motion of two mirrors in the cavity have two modes. One is differential motion, which is the length change of that. Another one is common motion, which is the motion of the center of the cavity. In terms of the length control, it is important that the RMS amplitude of differential motion is as small as possible. Actuarlly, the amplitude of these two motions are the same each other when the mirrors moves with no coherence. However, when a coherence exists, the common motion tends to be larger than the differential one.

As discussed in this section, the coherence depends on both, the arm length and the wavelength of seismic waves. For example, if the arm length is much more smaller than the wavelength, the mirrors move together. This means that the common motion is greater than the differential motion.

The ratio of the amplitudes of the differential motion over common motion is newly defined as Common and Differential Motion Ratio (CDMR). It is usefull to know how the ground reducts the differential motion or increase the common motion.

1.3.2 Differential Motion Reduction

Differential Motion and Common Motion

Motions of the two points can be represented as the differential motion and the common motion. Displacement of both differential motion and common motion of the two points shown in Figure(??) are defined as

$$u_{\text{diff}} \equiv \frac{u_1 - u_2}{\sqrt{2}}, \quad u_{\text{comm}} \equiv \frac{u_1 + u_2}{\sqrt{2}} \quad (1.2)$$

where $u_1(x, t)$ and $u_2(x, t)$ are the displacement of each points. These two motions defined in Eq.(1.2) are normalized by $\sqrt{2}$ due to conserve the total power.

Common and Differential Motion Ratio (CDMR)

CDMR is defined as the powers of common motion over the differential motion as bellow,

$$\text{CDMR} \equiv \sqrt{\frac{\text{Common Motion}}{\text{Differential Motion}}} = \sqrt{\frac{P_{\text{comm}}(\omega)}{P_{\text{diff}}(\omega)}} \quad (1.3)$$

where $P_{\text{comm}}, P_{\text{diff}}$ are the power spectral densities (PSDs) of the differential motion and common motion, respectively. Each PSDs are converted from the autocorrelation function of these by the Wiener-Khinchin theorem.

First, autocorrelation function C_{diff} of the differential motion is given by its definition in Eq.(1.2)

$$C_{\text{diff}}(\tau) = \frac{1}{2} \left\langle \left[x_1(t) - x_2(t) \right] \left[x_1(t + \tau) - x_2(t + \tau) \right] \right\rangle \quad (1.4)$$

$$= \frac{1}{2} \left[C_{11}(\tau) - C_{12}(\tau) - C_{21}(\tau) + C_{22}(\tau) \right], \quad (1.5)$$

, where C_{ij} are the autocorrelation functions of each point and defined as $C_{ij} \equiv \langle x_i(t)x_j(t+\tau) \rangle$, ($i = 1, 2, j = 1, 2$). Therefore, the power spectrum density of differential motion $P_{\text{diff}}(\omega)$ can be computed as

$$P_{\text{diff}}(\omega) = \frac{1}{2} \left[P_1(\omega) + P_2(\omega) - P_{12}(\omega) - P_{12}^*(\omega) \right] \quad (1.6)$$

$$= \frac{1}{2} \left[P_1 + P_2 - \text{Re} [\gamma] \times 2\sqrt{P_1 P_2} \right] \quad (1.7)$$

where $P_1(\omega), P_2(\omega)$ are the power spectrum densities of each points, and $P_{12}(\omega)$ are the cross spectrum between two point. The parameter γ is the complex coherence between them defined below,

$$\gamma \equiv \frac{P_{12}}{\sqrt{P_1 P_2}}. \quad (1.8)$$

Here, assuming that seismic wave propagating each points does not decay, which means $P_1 = P_2 \equiv P$, one can compute the $P_{\text{diff}}(\omega)$ as

$$P_{\text{diff}}(\omega) = P(1 - \text{Re} [\gamma]). \quad (1.9)$$

Therefore, the PSDs of the common motion can be calculated as

$$P_{\text{comm}}(\omega) = P(1 + \text{Re} [\gamma]). \quad (1.10)$$

Finally, CDMR defined Eq.(1.3) in case the seismic wave does not decay is represented as

$$\text{CDMR} = \sqrt{\frac{1 + \text{Re} [\gamma]}{1 - \text{Re} [\gamma]}}. \quad (1.11)$$

Eq.(1.11) indicate that CDMR can be expressed by only the coherence γ between of two points. For example, CDMR tends to be larger when γ close to 1. This means that the differential motion is more less than the common motion because the two points move together in the same direction.

1.4 Measurement of Differential Motion Reduction

1.4.1 Overview



Figure 1.8: Seismometers for measurement of the differential motion reduction

1.4.2 Reduction in X-arm Scale

図 1.6 に示すように、X アームの両端においた 2 台の地震計の信号をつかって X アームでの逆走低減効果を評価した。



Figure 1.9: ...

1.4.3 Reduction in Other Short Scale



Figure 1.10: ...

1.5 Summary of the Chapter



NO IMAGE

Figure 1.6

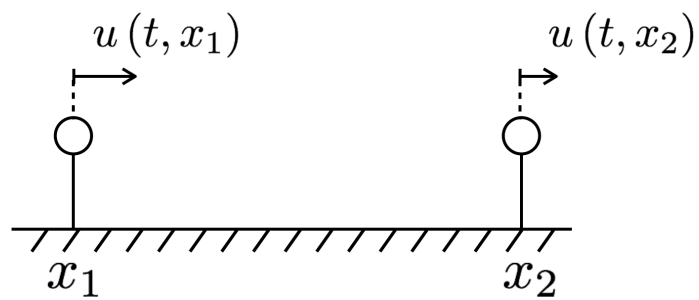


Figure 1.7: The displacements of the two points which are separated L in X axis.

Bibliography

- [1] Akiteru Takamori. *Low frequency seismic isolation for gravitational wave detectors*. PhD thesis, Department of Physics School of Science, University of Tokyo, 2002.
- [2] Takanori Sekiguchi. *A Study of Low Frequency Vibration Isolation System for Large Scale Gravitational Wave Detectors*. PhD thesis, Department of Physics School of Science, University of Tokyo, 2016.
- [3] Okutomi Koki. *Development of 13.5-meter-tall Vibration Isolation System for the Main Mirrors in KAGRA*. PhD thesis, SOKENDAI, The Graduate University for Advanced Studies, 2019. [Link](#).
- [4] Jerry A Carter, Noel Barstow, Paul W Pomeroy, Eric P Chael, and Patrick J Leahy. High-frequency seismic noise as a function of depth. *Bulletin of the Seismological Society of America*, 81(4):1101–1114, 1991.
- [5] LCGT collaboration. Lcgt design document version 3.0. Technical Report JGW-T0400030-v4, Institute for Cosmic Ray Research, University of Tokyo, JGW document, 11 2009.
- [6] Sylvette Bonnefoy-Claudet, Fabrice Cotton, and Pierre-Yves Bard. The nature of noise wavefield and its applications for site effects studies: A literature review. *Earth-Science Reviews*, 79(3-4):205–227, 2006.
- [7] Shuichi Sato, Shinji Miyoki, Souichi Telada, Daisuke Tatsumi, Akito Araya, Masatake Ohashi, Yoji Totsuka, Mitsuhiro Fukushima, Masa-Katsu Fujimoto, LISM Collaboration, et al. Ultrastable performance of an underground-based laser interferometer observatory for gravitational waves. *Physical Review D*, 69(10):102005, 2004.
- [8] P Bormann. New manual of seismological observatory practice. *GFZ German Research Centre for Geosciences*, 2012. [Link](#).
- [9] RA Haubrich, WH Munk, and FE Snodgrass. Comparative spectra of microseisms and swell. *Bulletin of the Seismological Society of America*, 53(1):27–37, 1963. [Link](#).
- [10] Michael Selwyn Longuet-Higgins. A theory of the origin of microseisms. *Philosophical Transactions of the Royal Society of London. Series A, Mathematical and Physical Sciences*, 243(857):1–35, 1950. [Link](#).

- [11] L Naticchioni, M Perciballi, F Ricci, E Coccia, V Malvezzi, F Acernese, F Barone, G Giordano, R Romano, M Punturo, R De Rosa, P Calia, and G Loddo. Microseismic studies of an underground site for a new interferometric gravitational wave detector. *Classical and Quantum Gravity*, 31(10):105016, may 2014.
- [12] Michael Coughlin, Christopher Stubbs, Sergio Barrientos, Chuck Claver, Jan Harms, R. Chris Smith, and Michael Warner. Real-time earthquake warning for astronomical observatories. *Experimental Astronomy*, 39(2):387–404, Jun 2015.
- [13] Michael Coughlin, Paul Earle, Jan Harms, Sebastien Biscans, Christopher Buchanan, Eric Coughlin, Fred Donovan, Jeremy Fee, Hunter Gabbard, Michelle Guy, Nikhil Mukund, and Matthew Perry. Limiting the effects of earthquakes on gravitational-wave interferometers. *Classical and Quantum Gravity*, 34(4):044004, feb 2017.
- [14] S Biscans, J Warner, R Mittleman, C Buchanan, M Coughlin, M Evans, H Gabbard, J Harms, B Lantz, N Mukund, A Pele, C Pezerat, P Picart, H Radkins, and T Shaffer. Control strategy to limit duty cycle impact of earthquakes on the LIGO gravitational-wave detectors. *Classical and Quantum Gravity*, 35(5):055004, jan 2018.
- [15] Jon R Peterson. Observations and modeling of seismic background noise. Technical report, US Geological Survey, 1993.
- [16] Nanometrics Inc., 250 Herzberg Road Kanata, Ontario, Canada K2K 2A1. *Trillium 120Q/QA User Guide*, 04 2017.
- [17] Rolf Bork, R Abbott, D Barker, and J Heefner. An overview of the ligo control and data acquisition system. *arXiv preprint physics/0111077*, 2001.